Desalination and Water Treatment
www.deswater.com

doi: 10.5004/dwt.2019.24782

171 (2019) 428–435
December

Preparation and characterization of MnO_2-impregnated granular activated carbon for Reactive Black 5 removal

Jianhai Zhao[a,*], Tingting Liu[a], Huanhuan Shi[a], Jiayi Zhang[a], Haiyan Li[b], Wenqi Ge[c], Yongzhi Chi[a]

[a]*Tianjin Key Laboratory of Aquatic Science and Technology, School of Environmental and Municipal Engineering, Tianjin Chengjian University, Tianjin 300384, China, Tel. +86 22-23085117; emails: jhzhao@tcu.edu.cn (J.H. Zhao), 1072491948@qq.com (T.T. Liu), 798875852@qq.com (H.H. Shi), 2820552116@qq.com (J.Y. Zhang), 23733403@126.com (Y.Z. Chi)*
[b]*Beijing Engineering Research Center of Sustainable Urban Sewage System Construction and Risk Control, Beijing University of Civil Engineering and Architecture, Beijing, China, email: lihaiyan@bucea.edu.cn*
[c]*School of Control and Mechanical Engineering, Tianjin Chengjian University, Tianjin, China, email: gewenqi@tcu.edu.cn*

Received 16 March 2019; Accepted 14 August 2019

ABSTRACT

Granular activated carbon (GAC) was impregnated with manganese dioxide through an impregnation-precipitation-calcination procedure for removing Reactive Black 5 (RB5) from aqueous solution. The higher Brunauer–Emmett–Teller surface areas (820.25 $m^2\ g^{-1}$) and porous structure were obtained for manganese dioxide-GAC. The X-ray diffractometer and scanning electron microscopy analysis revealed that a large amount of manganese dioxide coating on the GAC surface. The optimized manganese dioxide-GAC preparation conditions were $Mn(NO_3)_2$ and Na_2CO_3 solutions of 0.5 mol L^{-1}, impregnating time of 5 h, calcining time of 3 h and calcining temperature of 360°C. The experimental results indicated that the pseudo-second-order kinetic equation can be used to describe the adsorption of RB5 on manganese dioxide-GAC. The highest removal capacity of RB5 from solution for manganese dioxide-GAC was 4.468 mg g^{-1}.

Keywords: Granular activated carbon; Manganese dioxide; Reactive Black 5 (RB5); Adsorption

1. Introduction

Textile dyeing is a high-water consumption industry contributes a major share to wastewater generation [1–3]. Reactive dyes are extensively used in the last few years due to their good performance, however, removing reactive dyes from wastewater is difficult because of their high solubility, complex aromatic structures and synthetic origin [4–7]. If they are not properly treated before discharge to the environment, dyes wastewater may cause public concern and legislation problems. Therefore, treating dyes wastewater to limit the standard concentration of the environmental regulatory authority before discharging into water bodies is necessary [8,9].

The conventional removal methods are widely used such as coagulation, precipitation, biodegradation, advanced oxidation and adsorption [10–14]. Adsorption has become one of the major industrially viable techniques for treating dyes and the most widely used adsorbent is activated carbon because of its large surface area, microporous structure, chemical stability and its regeneration ability [15,16]. In spite of its widespread use for color removal, activated carbon remains expensive, high contact time, low adsorption capacity and difficult to regenerate. Therefore, the development of low-cost alternative adsorbents should be significant for the practical application of adsorption. For this reason, many researchers were focusing on activated carbon surface

* Corresponding author.

modification which can improve its surface characteristics to obtain better adsorption capacity.

The conventional modified methods for activated carbon include chemical and physical, such as traditional alkaline treatment, thermal treatment, sol-gel, impregnation, co-precipitation [17–21]. Calcination has a remarkable effect on the type, distribution, and contents of surface hydrated species. It influences key reactive sites for various surface reactions, and it also causes the removal of pollutants [22]. Manganese dioxide is a well-known material as adsorbents, catalysts, and catalyst support because of its high surface reactivity, adsorption capacity and oxidation ability [23,24]. Although the use of manganese dioxide (MnO_2) modified adsorbents has been reported widely, the focus has mainly been on the adsorption effect but there was little information on the effect of MnO_2 on the adsorption properties of active carbons. Moreover, the removal mechanism of MnO_2-granular activated carbon (GAC) and the oxidation role of MnO_2 in the adsorbent have been ignored.

The main objectives of the presented work focused on the preparation of MnO_2-GAC by impregnation, precipitation and calcination methods and adsorption of RB5 from aqueous solution. The characterization of the adsorbent was analyzed by scanning electron microscopy (SEM), Brunauer–Emmett–Teller (BET), thermogravimetric, X-ray diffraction (XRD) analysis and adsorption mechanisms were discussed. The impact of initial impregnating concentration on adsorption capacity and adsorption kinetic studies were also investigated.

2. Experimental setup

2.1. Materials

Stock solutions of $Mn(NO_3)_2$ and Na_2CO_3 were prepared by dissolving reagent grade metal nitrate salts, $Mn(NO_3)_2$ (Tianjin Guangfu) and Na_2CO_3 (Tianjin wind ship) in distilled water, respectively. Reactive Black 5 (RB5) belongs to azo dyes purchased from Tianjin Dongya Company. The molecular structure of RB5 is shown in Fig. 1.

Commercial coconut shell GAC which supplied from central water purification materials limited company (Henan, China) was used as sorbent material.

2.2. Preparation of adsorbents

2.2.1. Chemical modification

Before the experiments, GAC (2.0–3.0 mm in diameter) was washed a few times with de-ionized water to remove the surface dust and possible impurities, dried at 90°C for 3 h till the constant weight was observed.

Impregnation and co-precipitation method was used in modified GAC, and controlling a range of impregnating solutions concentration (0.1–1.3 mol L^{-1} $Mn(NO_3)_2$, impregnating time 5 h at room temperature. Then, the GAC supported manganese ions were separated and reacted with the same concentration of $NaCO_3$ for 5 h. After filtering, washing and drying, eventually, getting activated carbon loaded with manganese compounds. The samples were nominated as $Mn(NO_3)_2$-GAC and $MnCO_3$-GAC, respectively. This method can not only make the manganese compounds homogeneous adhere to the surface of GACs, but also make them entering into the pore structure of GACs, increasing manganese attachment sites. The reaction equation is as follows:

$$Mn(NO_3)_2 + Na_2CO_3 = MnCO_3 \downarrow + 2NaNO_3 \quad (1)$$

2.2.2. Calcination

After GAC impregnated manganese, secondly, start to calcination process, which is similar to the carbonization and activation of the GAC preparation process. The samples were prepared by calcining temperature 360°C and calcining time 3.5 h in a muffle furnace. The samples were nominated as MnO_x-GAC and MnO_2-GAC, respectively. $Mn(NO_3)_2$ and $MnCO_3$ thermal decomposition by calcining, reaction equations are as follows:

$$MnCO_3 \rightarrow MnO + CO_2 \uparrow \quad (2)$$

$$2MnO + O_2 \rightarrow 2MnO_2 \quad (3)$$

$$Mn(NO_3)_2 \rightarrow MnO_x + NO \uparrow \quad (4)$$

All kinds of products were stored for future use. The specific preparation steps as shown in Fig. 2.

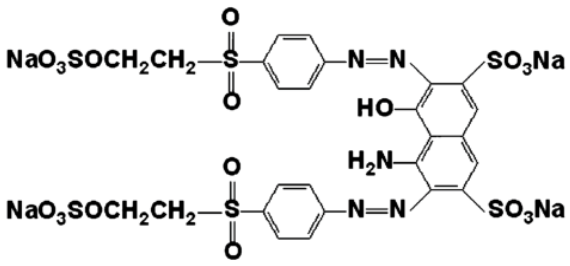

Fig. 1. Molecular structure of Reactive Black 5.

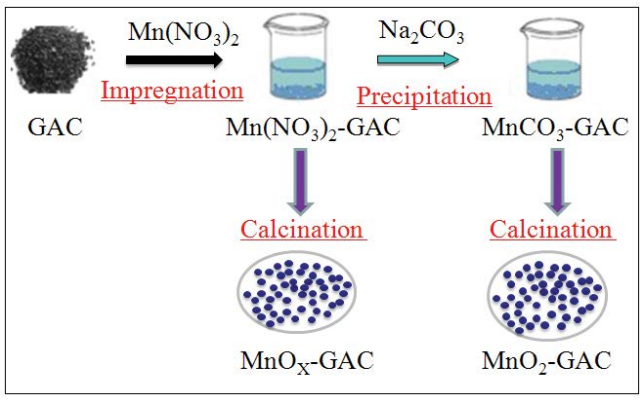

Fig. 2. Preparation process of modified GAC.

2.2.3. Characterization

Firstly, the manganese content of modified GAC was selected by the microwave digestion system (ETHOSE, Milestone, Italy). 0.5 g modified MnO_2-GACs and 10 mL HNO_3 added into digestion tanks, then digested 40 min, cooled, filtered and diluted to allow measure range of inductively coupled plasma mass spectrometry (ICP-MAS) (Agilent 7000E, USA). Finally, the manganese concentrations were analyzed using ICP-MAS.

Modified GACs chemical compositions and crystallization were probed using XRD (vctima IV, Rigaku Corporation, Japan). GACs surface morphology, microstructure, and elemental distribution were investigated by SEM using a JSM-7800F SEM (Quanta 200, FEI, Czech). N_2 adsorption was performed on each adsorbent using a nitrogen gas adsorption analyzer (ASAP 2020, Micromeritics, USA). The N_2 adsorption on the samples was used to calculate the specific surface area using the BET equation.

2.2.4. Adsorption experiments

Adsorption of RB5 was carried out by batch experiments. 100 mL of 50 mg L^{-1} RB5 was taken in 250 mL conical flask and the same amount of 0.5 g of adsorbents was added into it shaking 3 h at 25°C until the establishment of equilibrium. The pH of the solution at 7.2 was not adjusted. It was carried out to examine the influence factors such as initial impregnating concentrations of $Mn(NO_3)_2$ and Na_2CO_3 for adsorption efficiency. The adsorption kinetics of RB5 (50 mg L^{-1}) on MnO_2-GAC was determined at the time intervals in the range of 1–11 h for at 25°C, pH at 7.2.

The suspensions were filtered using a 0.45 μm filter paper, and the concentration of the filtrate of RB5 in the solution was analyzed by a UV-VISIBLE spectrophotometer (UV2550 Shimadzu, Japan). The measurements were made at the wavelength of 598 nm, which corresponds to maximum absorbance. The differences between the initial and the equilibrium RB5 concentrations determine the amount that RB5 adsorbed by adsorbents. The adsorption amount at equilibrium was calculated by mass balance using the following equation:

$$Q_e = \frac{(C_0 - C_e)V}{m} \quad (5)$$

where Q_e is sorption capacity at equilibrium (mg g^{-1}), V is the volume of RB5 solution taken (mL), C_0 and C_e are the initial and equilibrium RB5 concentration (mg L^{-1}), respectively, and m is mass of adsorbent used (g).

3. Results and discussion

3.1. Characterization of MnO_2-GAC

3.1.1. Thermal analysis

MnO_2-GAC was prepared under such conditions: 0.5 mol L^{-1} of $Mn(NO_3)_2$ and Na_2CO_3, impregnating time of 5 h, calcining time of 3 h and temperature of 360°C. Fig. 3 shows the thermogravimetric curves (TGA) of the thermal decomposition process of MnO_2-GAC obtained at a heating rate of 10°C min^{-1} in the air from room temperature to

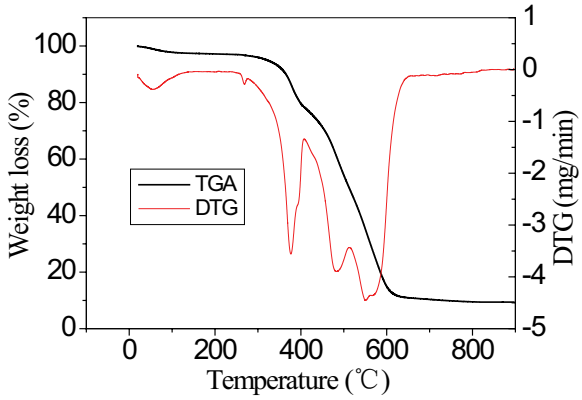

Fig. 3. TGA and DTG curves of MnO_2-GAC.

900°C. TGA curves included a relatively stable phase and a rapid mass loss phase, the total weight loss of the MnO_2-GAC was corresponding to 90.6%. The first weight loss occurs during the heating step from 60°C to 280°C, corresponding to 3.5%. The derivative thermogravimetric curve (DTG) of MnO_2-GAC shows an exothermic peak at 90°C, it can be attributed to the release of water molecules which sorbed on the solid surfaces and also inside the lamellar cavity [25]. While the second mass loss process, weight loss about for 17% was observed from 300°C to around 400°C. The DTG curve revealed a strong *exothermic peak* at 360°C which was probably due to the decomposition of $MnCO_3$ during the healing process, along with forming the manganese oxides. The third and fourth exothermic peak at 470°C and 550°C on this curve may be due to the decomposition of manganese oxides which included the auto-combustion of MnO_2-GAC to end in the final residue [26]. Thermal transformation and thermogravimetric characteristics of different manganese oxides under inert and air atmosphere had been studied in the literature and the author found that pyrolusite (MnO_2) exhibited weight loss from around 60°C, and rapid weight loss starts from below 600°C under inert atmosphere [27,28]. Less weight loss above 600°C indicated the final collapse of the MnO_2-GAC structure ended with residue.

3.1.2. BET characterization

Nitrogen isotherms were used to compare the specific surface areas and pore structures of the samples. The nitrogen isotherm adsorption of GAC and MnO_2-GAC are shown in Fig. 4. According to the International Union of Pure and Applied Chemistry (IUPAC) classification, GAC and MnO_2-GAC materials exhibited the characteristic of Types I [29]. Type I isotherm exhibits significant adsorption at low relative pressures and is due to the micropores adsorption. As shown in Fig. 4, the N_2 isotherms of MnO_2-GAC exhibited a greater slope than that of GAC, which indicated higher adsorption by MnO_2-GAC.

The physical parameters of GAC such as BET specific surface area (S_{BET}), total pore volume (V_t), average pore diameter (D_p) mentioned in Table 1. As seen from Table 1, GAC possesses a high specific surface area (707.55 m^2 g^{-1}), and pore volume (0.130 cm^3 g^{-1}), which indicated it can be

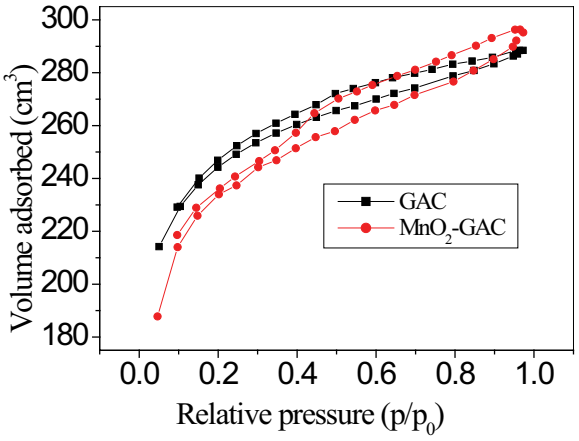

Fig. 4. Volume of N_2 adsorption isotherm versus pressure for GAC and MnO_2-GAC.

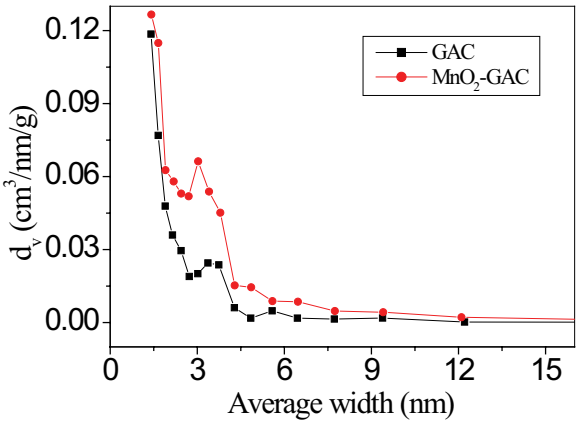

Fig. 5. Pore size distribution of GAC and MnO_2-GAC.

Table 1
Porous structure parameters of activated carbons

Adsorbents	S_{BET} ($m^2\ g^{-1}$)	V_t ($cm^3\ g^{-1}$)	D_p (nm)
GAC	707.55	0.130	1.405
MnO_2-GAC	820.25	0.270	1.436

a potential adsorbent. Furthermore, when the impregnating concentrations were less than 0.5 mol L^{-1}, the BET surface areas were increased from 707.55 $m^2\ g^{-1}$ for GAC to 820.25 $m^2\ g^{-1}$ for MnO_2-GAC because the MnO_2-GAC surface was relatively evident and denser than on GAC surfaces. However, when the impregnating concentrations increased to 0.7 mol L^{-1}, the BET surface areas decreased to 735.11 $m^2\ g^{-1}$. This means that too much formation of the disordered pore structure of MnO_2 will change the texture properties of MnO_2-GAC and consequently resulting in a lower adsorption capacity [30]. The same trend was also true for the change in total pore volume and average pore diameter.

One of the significant properties of GAC is the pore size distribution, which determines the fraction of the total pore volume accessible to molecules of a given size and shape [31]. This can be seen from Fig. 5, according to the IUPAC classification of pore dimensions, the pores of absorbents can be classified as micropores (d < 2 nm), mesopores (d = 2–50 nm), and macropores (d > 50 nm). Fig. 5 indicates that MnO_2-GAC included a large number of micropores and some mesopores and that MnO_2-GAC contains greater mesopores than GAC. This high mesopores content could be attributed to the heating method due to removing impurities and the formation of the new structure from the surface to the inside of MnO_2-GAC [32].

3.1.3. SEM characterization

The SEM is the primary tool used for characterization of the surface morphology and fundamental physical properties such as particle size, shape, and porosity of GACs surface. Morphology and microstructure of the GACs (Fig. 6) according to SEM studies reveal that the raw coconut shell GAC (Fig. 6a) generally had a cave-like shape with the highly porous structure or voids over a large area. Coconut shell GAC was suitable for trapping and adsorption of dyes into these pores. According to the SEM images, after calcining at 360°C for 3 h, residual volatile substances discharged and the original pore expanded, so that MnO_2-GAC has become a good structure of porous material. Furthermore, it can also be seen from the SEM image of MnO_2-GAC (Fig. 6b) that cluster-cluster aggregation of hexahedron and octahedron particles adhering onto its surface, which implied that MnO_2 formed within the calcination [30].

Therefore, known from the analysis of SEM images, 0.5 mol L^{-1} of $Mn(NO_3)_2$ and Na_2CO_3, impregnating time of 5 h, calcining time of 3 h and temperature of 360°C were chosen to the optimize MnO_2-coating on the GAC and this was used for the latter experimental process. After adsorption, significant changes observed in the surface morphology of dye-loaded MnO_2-GAC (Fig. 6c) indicated the existent of dyes molecular cloud on the surface and pore.

3.1.4. XRD characterization

To evaluate the species of impregnated manganese, modified GACs were analyzed by XRD analyses and compared to purity GAC as shown in Fig. 7. The sharp peaks at 2θ = 26° corresponded to graphite structure [33]. It was noticed that the XRD pattern of the MnO_2-GAC sample was more crystalline than raw GAC. MnO_2-GAC diffraction patterns showed that d-spacings were 4.924, 3.078, 2.758, 2.488, 2.032, 1.576 Å (Fig. 7), which diffraction peaks at 2θ values of 17.890°, 29.043°, 32.514°, 36.090°, 44.714°, and 58.597°, respectively. All these broader and weaker diffraction peaks were ascribed to the formation of the MnO_2 crystalline phase [34]. Furthermore, no characteristic peaks of other crystalline impurities were detected by XRD in all samples, suggesting that the product was pure manganese oxide with a space group of MnO_2-GAC. So, manganese dioxide acted as convenient support to GAC.

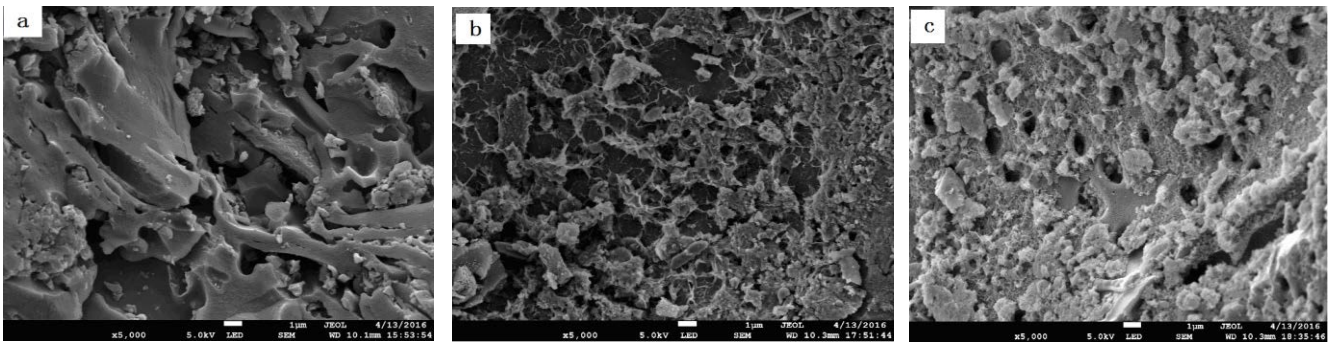

Fig. 6. SEM images of GAC_s (a) GAC, (b) MnO_2-GAC, and (c) MnO_2-GAC after adsorption.

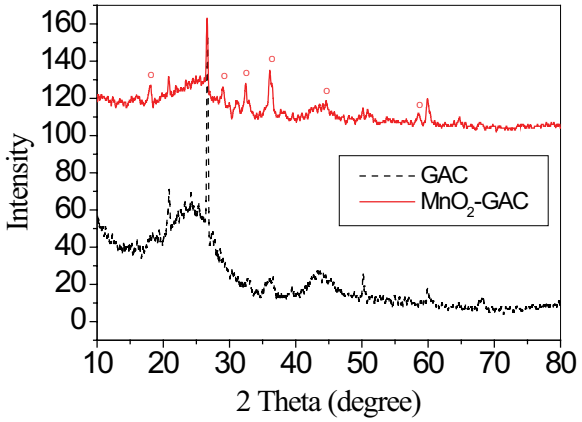

Fig. 7. XRD pattern of GAC and MnO_2-GAC.

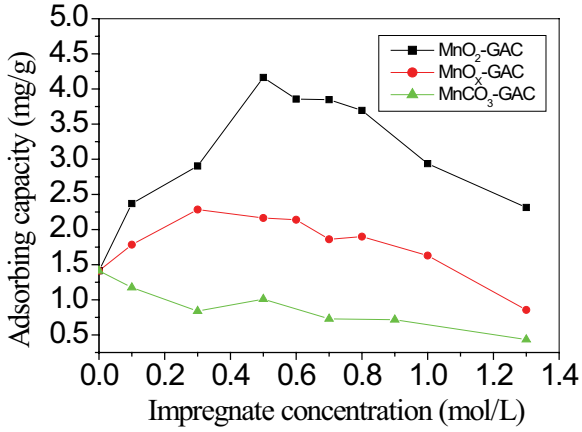

Fig. 8. Adsorption capacity of GACs with different impregnate concentration

3.2. Adsorption Results

3.2.1. Influence of impregnating solution concentration

The amount of MnO_2 on GAC can play an important role in the whole preparation process. To investigate the influence of the MnO_2 on GAC removal dyes capacities, water solutions with given MnO_2 were prepared at different $Mn(NO_3)_2$ and Na_2CO_3 of initial concentration in the range between 0.1 and 1.3 mol L^{-1} which are presented in Fig. 8. From Fig. 8, it was observable that the maximum removal efficiency occurred at 0.5 mol L^{-1}. Subsequently, the adsorption capacity decreased as the initial solution concentration increased from 0.5 to 1.3 mol L^{-1}. The main reason for this phenomenon may be the greater availability of adsorption sites initially, and RB5 can contact the effective adsorption sites on the modified GAC rapidly. After being adsorbed on the particle surface or interspace sites, physical or chemical forces occurred between the RB5 and the manganese dioxides and GAC [35,36]. However, as the impregnating process, the higher $Mn(NO_3)_2$ and Na_2CO_3 concentrations competed with RB5 for limited adsorption sites, which were not in favor of RB5 adsorption by MnO_2-GAC. Table 2 shows the manganese contents of MnO_2-GACs which were prepared with $MnCO_3$ concentrations of 0.3, 0.5, 0.7 mol L^{-1}, respectively, impregnating time of 5 h, calcining time of 3 h, the calcining temperature of 360°C. The samples were nominated as MnO_2-GAC_1, MnO_2-GAC_2, MnO_2-GAC_3. As can be seen, the manganese content of MnO_2-GACs increased as the concentration of manganese increased. Thus, the adsorbing capacity of MnO_2-GAC was greater at lower initial concentrations and smaller at higher initial concentrations. This suggests that the MnO_2-GAC surface was rebuilt new structures by MnO_2 in low impregnating concentrations. This result showed that adsorption sites will be saturated through the impregnation process with a higher MnO_2 amount. Based on these results, 0.5 mol L^{-1} of $Mn(NO_3)_2$ and Na_2CO_3 were used in further experiments. The removal efficiency of 50 mg L^{-1} RB5 within 3 h can be ranked as MnO_2-GAC, MnO_x-GAC, $MnCO_3$-GAC.

Table 2
Manganese content of MnO_2-GACs

MnO_2-GACs	MnO_2-GAC_1	MnO_2-GAC_2	MnO_2-GAC_3
Impregnating manganese concentration (mol L^{-1})	0.3	0.5	0.7
Manganese content of MnO_2-GAC (mg g^{-1})	17.74	27.86	38.99

3.2.2. Adsorption kinetics

The adsorption kinetics is one of the most important characters because it can demonstrate the solute uptake rate of dyes from aqueous solutions by the adsorbents and therefore, determines their potential applications. As seen in Fig. 9, the kinetics of RB5 adsorption onto modified adsorbents obtained by 1–11 h shaking for a dye concentration of 50 mg L^{-1} at pH 7.2. According to Fig. 9, under the same experimental conditions, GAC, MnO_2-GAC adsorption results revealed that adsorption processes were clearly time-dependent such that a dramatical increase of the capacity of RB5 removal, and they reached equilibrium gradually at first 9 h, 6 h, follow-up of a slow increase until reaching adsorption equilibrium at 10 h, 8 h, respectively. Furthermore, MnO_2-GAC has the fastest dyes uptake rate and highest adsorption capacity, where the equilibrium adsorption quantity is 4.468 mg g^{-1} for MnO_2-GAC and twice than that of GAC (2.419 mg g^{-1}), respectively. This phenomenon is because of their higher specific surface areas and pore size as well as unique microporous structures [37].

To analyze the rate-controlling and mass transfer mechanism of the adsorption process, experimental kinetic data were analyzed according to linear forms of two well-known kinetic models [37]. Firstly, the pseudo-first-order kinetic model has been widely used to predict sorption kinetics. The model was shown below as Eq. (6).

$$\ln(q_e - q_t) = \ln q_e - k_1 t \tag{6}$$

where q_e and q_t were the adsorption capacity of dye adsorbed (mg g^{-1}) at equilibrium and at time t, respectively, and k_1 (min^{-1}) was the rate constant of adsorption. Values of k_1 were calculated from the plots of ln ($q_e - q_t$) versus t (Fig. 10a) for the three samples.

The correlation coefficient R^2 values obtained were 0.758, 0.902 for GAC, MnO_2-GAC, and the experimental q_e values showed disagreement with the calculated values obtained from the linear plots (Table 3), indicating the poor correlation coefficients for the first-order model of the adsorption process.

Secondly, the pseudo-second-order equation based on experimental data was evaluated by Eq. (7).

$$\frac{t}{q_e} = \frac{1}{k_2 q_e^2} + \frac{t}{q_e} \tag{7}$$

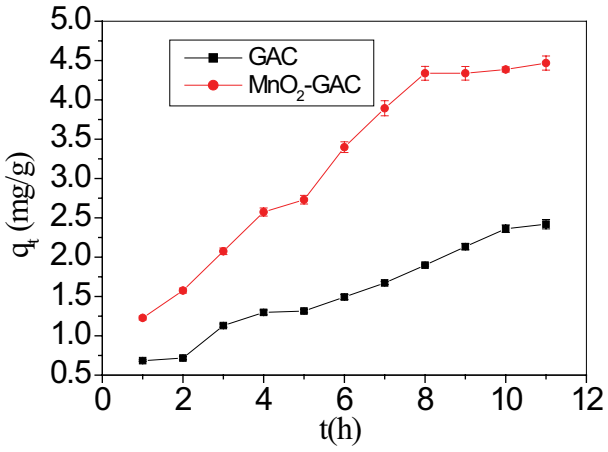

Fig. 9. Adsorption of RB5 on GAC and MnO_2-GAC.

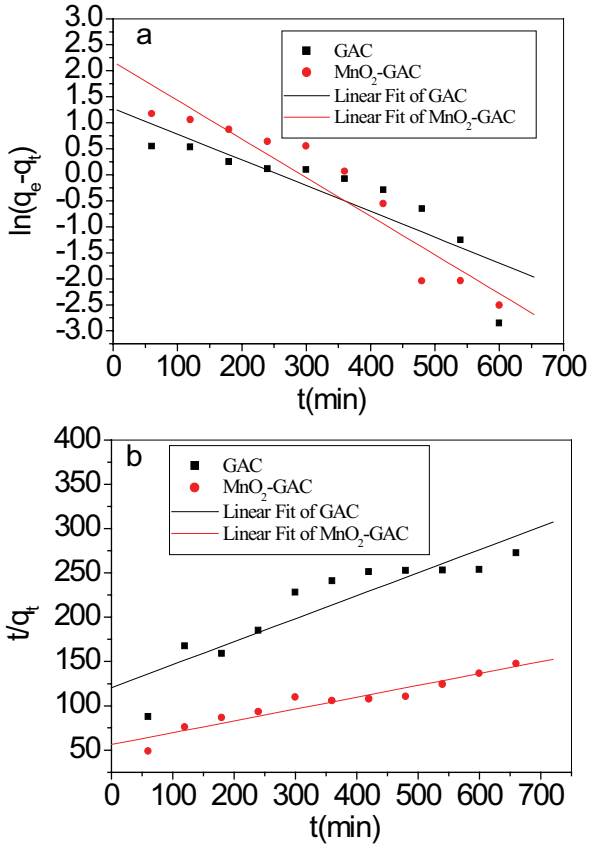

Fig. 10. Adsorption kinetics of RB5 on GAC and MnO_2-GAC (a) pseudo-first-order kinetics and (b) pseudo-second-order kinetics.

Table 3
Fitted kinetic parameter for the adsorption of RB5 onto GAC_S

			Pseudo-first-order model		Pseudo-second-order model	
Sample	C_0 (mg L^{-1})	$q_{e,exp}$ (mg g^{-1})	$q_{e,cal}$ (mg g^{-1})	R^2	$q_{e,cal}$ (mg g^{-1})	R^2
GAC	50	2.419	3.586	0.758	3.856	0.823
MnO_2-GAC	50	4.468	8.782	0.902	7.480	0.917

where q_e and q_t were the adsorption capacity of dye adsorbed (mg g^{-1}) at equilibrium and at any time t, k_2 (g (mg min)$^{-1}$) was the pseudo-second-order rate constant.

The linear plot of t/q_t vs. t is shown in Fig. 10b and the R^2 values calculated from the slopes and intercepts are summarized in Table 3. It was clear that the experimental q_e values agreed with the calculated values obtained from the linear plots (Table 3). Based on the high degree of correlation coefficient of 0.823, 0.917 for GAC, MnO_2-GAC, respectively. It suggested that the pseudo-second-order equation was adequate in describing the adsorption kinetics of RB5 on MnO_2-GAC. The pseudo-second-order model suggests that the adsorption depends on the adsorbate as well as the adsorbent and involves chemisorption and physisorption processes [14].

4. Conclusion

A new adsorbent, MnO_2 modified GAC was prepared with a large specific surface area and pore volume. The optimized manganese dioxide-GAC preparation condition was identified based on RB5 adsorption efficiency. The pseudo-second-order adsorption kinetics modeling can better describe the adsorption of RB5 on MnO_2-GAC. The excellent adsorption capacity of 4.468 mg g^{-1} from aqueous solutions was achieved in a short time (3 h) under optimum conditions. Based on a favorable removal performance, the modification process was confirmed to be useful and MnO_2-GAC can be used as a novel and promising adsorbent material to treat contaminated water with reactive dyes.

Acknowledgement

The authors would like to acknowledge the support of the State Key Laboratory of Chemical Engineering (SKL-ChE-13C03) and Beijing Great Wall Scholars Program (CIT&TCD20170313).

References

[1] A.K. Verma, R.R. Dash, P. Bhunia, A review on chemical coagulation/flocculation technologies for removal of colour from textile wastewaters, Environ. Manage., 93 (2012) 154–168.
[2] T. Fazal, A. Mushtaq, F. Rehman, A.U. Khan, N. Rashid, W. Farooq, M.S.U. Rehman, J. Xu, Bioremediation of textile wastewater and successive biodiesel production using microalgae, Renewable Sustainable Energy Rev., 82 (2017) 3107–3126.
[3] F. Abiri, N. Fallah, B. Bonakdarpour, Sequential anaerobic-aerobic biological treatment of colored wastewaters: case study of a textile dyeing factory wastewater, Water Sci. Technol., 75 (2017) 1261–1269.
[4] F. Gomri, M. Boutahala, H. Zaghouane-Boudiaf, S.A. Korili, A. Gil, Removal of acid blue 80 from aqueous solutions by adsorption on chemical modified bentonites, Desal. Wat. Treat., 57 (2016) 1–10.
[5] H.Y. Li, S.Y. Liu, J.H. Zhao, N. Feng, Removal of reactive dyes from wastewater assisted with kaolin clay by magnesium hydroxide coagulation process, Colloids Surf., A, 494 (2016) 222–227.
[6] W. Handayani, A.I. Kristijanto, A.I.R. Hunga, Are natural dyes eco-friendly? A case study on water usage and wastewater characteristics of batik production by natural dyes application, Sustainable Water Resour. Manage., 3 (2018) 1–11.
[7] M. Tinkara, L. Aleksandra, M. Gerhard, T. Matejka, Design and characterization of dicyanovinyl reactive dyes for the colorimetric detection of thiols and biogenic amines, Sensors, 18 (2018) 1–13.
[8] M.E. Karim, K. Dhar, M.T. Hossain, Decolorization of textile reactive dyes by bacterial monoculture and consortium screened from textile dying effluent, Genet. Eng. Biotechnol. News, 16 (2018) 375–380.
[9] W.T. Mook, M.K. Aroua, M. Szlachta, Palm shell-based activated carbon for removing reactive black 5 dye: equilibrium and kinetics studies, Bioresources, 11 (2016) 1432–1447.
[10] H.S. Saroyan, D.A. Giannakoudakis, C.S. Sarafidis, N.K. Lazaridis, E.A. Deliyanni, Effective impregnation for the preparation of magnetic mesoporous carbon: application to dye adsorption, Chem. Technol. Biotechnol., 92 (2017) 1899–1911.
[11] M. Abbasi, Synthesis and characterization of magnetic nanocomposite of chitosan/SiO_2/carbon nanotubes and its application for dyes removal, J. Cleaner Prod., 145 (2017) 105–113.
[12] A. Yurtsever, E. Sahinkaya, E. Aktaş, D. Uçar, O. Cınar, Z. Wang, Performances of anaerobic and aerobic membrane bioreactors for the treatmentof synthetic textile wastewater, Bioresour. Technol., 192 (2015) 564–573.
[13] W.F. Khalik, L.N. Ho, S.A. Ong, Y.S. Wong, N.A. Yusoff, F. Ridwan, Solar photocatalytic mineralization of dye new coccine in aqueous phase using different photocatalysts, Water Air Soil Pollut., 227 (2016) 1–8.
[14] M.E.I. Haddad, A. Regti, M.R. Laamari, R. Slimani, R. Mamouni, S.E.I. Antri, S. Lazar, Calcined mussel shells as a new and eco-friendly biosorbent to remove textile dyes from aqueous solutions, J. Taiwan Inst. Chem. Eng., 45 (2014) 533–540.
[15] H. Al-Johani, M.A. Salam, Kinetics and thermodynamic study of aniline adsorption by multi-walled carbon nanotubes from aqueous solution, Colloid Interface Sci., 360 (2011) 760–767.
[16] H.A. Ahsaine, M. Zbair, Z. Anfar, Y. Naciri, R. El Haouti, N. El Alem, M. Ezahri, Cationic dyes adsorption onto high surface area 'almond shell' activated carbon: kinetics, equilibrium isotherms and surface statistical modeling, Mater. Today Chem., 8 (2018) 121–132.
[17] I. Enniya, L. Rghioui, A. Jourani, Adsorption of hexavalent chromium in aqueous solution on activated carbon prepared from apple peels, Sustainable Chem. Pharm., 7 (2018) 9–16.
[18] Y.F. Pan, C.T. Chiou, T.F. Lin, Erratum to: adsorption of arsenic(V) by iron-oxide-coated diatomite (IOCD), Environ. Sci. Pollut. Res. Int., 17 (2010) 1401–1410.
[19] C. Boruban, E.N. Esenturk, Activated carbon-supported CuO nanoparticles: a hybrid material for carbon dioxide adsorption, J. Nanopart. Res., 20 (2018) 59.
[20] W. Suprun, M. Lutecki, R. Gläser, H. Papp, Catalytic activity of bifunctional transition metal oxide containing phosphated alumina catalysts in the dehydration of glycerol, J. Mol. Catal. A: Chem., 342 (2011) 91–100.
[21] S. Babay, T. Mhiri, M. Toumi, Synthesis structural and spectroscopic characterizations of maghemite γ-Fe_2O_3 prepared by one-step coprecipitation route, J. Mol. Struct., 1085 (2015) 286–293.
[22] Y.P. Yuan, D. Liu, D.Y. Tan, K.K. Liu, H.G. Yu, Y.H. Zhong, A.H. Yuan, W.B. Yu, H.P. He, Surface silylation of mesoporous/macroporous diatomite (diatomaceous earth) and its function in Cu(II) adsorption: the effects of heating pretreatment, Microporous Mesoporous Mater., 170 (2013) 9–19.
[23] Y. Du, L. Wang, J. Wang, G. Zheng, J. Wu, H. Dai, Flower-, wire-, and sheet-like MnO_2-deposited diatomites: highly efficient absorbents for the removal of Cr(◎), Environ. Sci., 29 (2015) 71–81.
[24] X.Z. Yu, D.H. Xiao, L. Fei, P.D. Zeng, Y.G. Zao, L. Jing, pH-depend degradation of methylene blue via rational-designed MnO_2 nanosheet-decorated diatomites, Ind. Eng. Chem. Res., 53 (2014) 6966–6977.
[25] A.S.O. Moscofian, C.T.G.V.M.T. Pires, A.P. Vieira, C. Airoldi, Organofunctionalized magnesium phyllosilicates as mono-or bifunctitonal entities for industrial dyes removal, RSC Adv., 2 (2012) 3502–3511.

[26] S. Wang, B. Gao, Y. Li, A. Mosa, A.R. Zimmerman, A.R. Ma, W.G. Harris. K.W. Migliaccio, Manganese oxide-modified biochars: Preparation, characterization, and sorption of arsenate and lead, Bioresour. Technol., 181 (2015) 13–17.
[27] C. González, J.I. Gutiérrez, J.R. González-Velasco, A. Cid, A. Arranz, J.F. Arranz, Transformations of manganese oxides under different thermal conditions, J. Therm. Anal., 47 (1996) 93–102.
[28] J. Zhang, D.G. Tang, H.W. Yang, H.M. Yang, Preparation of dimanganese trioxide by decomposing manganese carbonate under high temperature, Shandong Chem. Ind., 42 (2013) 1–4 (In Chinese).
[29] K.S.W. Sing, Reporting physisorption data for gas/solid systems with special reference to the determination of surface area and porosity, Pure Appl. Chem., 54 (1982) 2201–2218.
[30] L. Jiang, L. Liu, S. Xiao, J. Chen, Preparation of a novel manganese oxide-modified diatomite and its aniline removal mechanism from solution, Chem. Eng. J., 284 (2016) 609–619.
[31] D. Hui, G. Zhang, X. Xu, G. Tao, J. Dai, Optimization of preparation of activated carbon from cotton stalk by microwave assisted phosphoric acid-chemical activation, J. Hazard. Mater., 182 (2010) 217–224.
[32] R.H. Hesas, A. Arami-Niya, M.A.W.D. Wan, J.N. Sahu, Preparation and characterization of activated carbon from apple waste by microwave-assisted phosphoric acid activation: application in methylene blue adsorption, Bioresources, 8 (2013) 2950–2966.
[33] Z.C. Kadirova, M. Hojamberdiev, K.I. Katsumata, T. Isobe, N. Matsushita, A. Nakajima, Preparation of iron oxide-impregnated spherical granular activated carbon-carbon composite and its photocatalytic removal of methylene blue in the presence of oxalic acid, J. Environ. Sci. Health., Part A, 49 (2014) 763–769.
[34] S. Wang, B. Gao, Y. Li, Y. Wan, A.E. Creamer, Sorption of arsenate onto magnetic iron–manganese (Fe–Mn) biochar composites, RSC Adv., 5 (2015) 67971–67978.
[35] N.F. Cardoso, E.C. Lima, I.S. Pinto, C.V. Amavisca, B. Royer, R.B. Pinto, W.S. Alencar, S.F.P. Pereira, Application of cupuassu shell as biosorbent for the removal of textile dyes from aqueous solution, Environ. Manage., 92 (2011) 1237–1247.
[36] B. Royer, N.F. Cardoso, E.C. Lima, T.R. Macedo, C. Airoldi, A useful organofunctionalized layered silicate for textile dye removal, J. Hazard. Mater., 181 (2010) 366–374.
[37] H.R. Mahmoud, S.A. El-Molla, M. Saif, Improvement of physicochemical properties of Fe_2O_3/MgO nanomaterials by hydrothermal treatment for dye removal from industrial wastewater, Powder Technol., 249 (2013) 225–233.